

Gravitational waves and primordial black holes from chirality imbalanced QCD first-order phase transition with \mathcal{P} and \mathcal{CP} violation

Jingdong Shao^{1,*} and Mei Huang^{2,†}

¹*School of Physics, University of Chinese Academy of Sciences, Beijing 100049, China*

²*School of Nuclear Science and Technology, University of Chinese Academy of Sciences, Beijing 100049, China*

The chirality imbalance in QCD is spontaneously induced by a repulsive axial-vector interaction from the instanton anti-instanton pairing at high temperature above the chiral phase transition, and vanishes at low temperature. Phase transition of the chirality imbalance is always a first-order one in the early universe with \mathcal{P} and \mathcal{CP} violation. The spectra of gravitational waves and the formation of the primordial black holes from this first-order phase transition is investigated in this work, and the effect of a strong magnetic field is also analyzed. The gravitational waves produced by chirality imbalance can be detected by LISA, Taiji and DECIGO, with the peak energy density locating in the range of 10^{-11} to 10^{-9} and the peak frequencies lying in the range of 10^{-5} Hz to 10^{-2} Hz. The spectrum with larger axial vector coupling strength and stronger magnetic field has higher peak energy density and lower peak frequency. According to this trend, the gravitational waves spectra might also be able to be detected by SKA, IPTA and EPTA. Based on the mechanism of postponement of the false vacuum decay, it is scarcely possible to form PBHs in our model with typical parameters because the phase transition completes in an extreme short time and thus the false vacuum energy density decays sharply.

CONTENTS

I. Introduction	1
II. Axial anomaly, chirality imbalance and first-order phase transition	3
III. Gravitational waves	5
IV. Primordial black holes	7
V. Summary and discussion	8
Acknowledgments	9
References	9

I. INTRODUCTION

In 1916, Albert Einstein predicted that gravitational waves (GWs) can be generated by the changes of the curvature of spacetime and propagate outwards at the speed of light [1, 2]. 100 years later, on February 11, 2016, the LIGO and Virgo Scientific Collaboration [3] announced the first observed GWs signal named GW150914 originated from a binary black hole merge. Then the GWs signal GW170817 originated from a binary neutron star inspiral was observed by LIGO in 2017 [4].

GWs can provide an unmodified record of cosmic events, therefore the observation of GWs opens a new exciting era for astronomy and cosmology. GWs can be

produced through compact binary inspirals and mergers, explosion of supernovae. Besides, it has been expected that the primordial GWs can be produced in the very early stages of the universe, which carry unique imprints on the cosmic microwave background. GWs also can be produced from cosmological phase transitions in the early universe through electroweak (EW) and Quantum Chromodynamics (QCD) phase transition, and these GWs can reveal the evolution of the universe.

Current and planned GW detector projects include pulsar timing arrays, as well as ground- and space-based interferometers in the frequency range between nHz and kHz. LIGO, VIRGO [5, 6] and the future Einstein Telescope (ET) [7, 8] are operating in the frequency range of 1 Hz to 10^4 Hz. 0.01–10 Hz frequency band can be covered by atom interferometers such as MAGIS ("mid-band" 30 mHz to 10 Hz) [9], AION (0.01 Hz to a few Hz) [10] and AEDGE [11] and the space-based mission the Big Bang Observer (BBO, 0.1–1 Hz) [12], DECIGO (deci-Hz, 0.1 Hz to 10 Hz) [13, 14], 10^{-4} –0.1 Hz frequency band can be covered by space-based interferometers Laser Interferometer Space Antenna (LISA) [15], Taiji [16, 17] and Tianqin [18]. The pulsar timing arrays (PTA) [19, 20] including NANOGrav [21], IPTA [22] and EPTA [23], and other radio telescopes including SKA project [24, 25] and the Five-Hundred-Meter Aperture Spherical Radio Telescope (FAST) project [26], can focus on the very-low-frequency GWs around 1–100 nHz through pulsar timing observation. GWs with much lower frequency have been expected to be detected through the polarization pattern of the cosmic microwave background [27] by primordial GW detectors, such as AliCPT [28], while GWs with much higher frequency covering regimes such as MHz and GHz, have been discussed in [29, 30]. Most of gravitational-wave observatories and their sensitivity frequencies and energy ranges are summarized in Ref. [29, 31, 32].

* shaojingdong19@mails.ucas.ac.cn

† huangmei@ucas.ac.cn

A strong first-order phase transition is required to produce GWs [33–36] through the nucleation and collision of true vacuum bubbles, such as first-order inflation, GUT symmetry breaking, EW symmetry breaking as well as QCD phase transition. There is no first-order phase transition in the standard model (SM), thus first-order phase transitions beyond the standard model have been explored [37], which is also a required condition for baryogenesis (BG) [38, 39].

The QCD phase transition, which is flavor and quark mass dependent [40], is rather complicated. There are two important phase transitions well defined in two extreme quark mass limits respectively, the chiral phase transition with the order parameter chiral condensation of light flavors and the deconfinement phase transition for the gluon system characterized by the order parameter of the Polyakov loop. In the chiral limit, the chiral phase transition is a second-order one in the 2-flavor case around $T_c = 175\text{MeV}$, and a first-order one in the 3-flavor case around $T_c = 155\text{MeV}$. The lattice calculation [41] shows that with physical quark mass, QCD phase transition at finite-temperature in the hot early universe is not a real phase transition, but a smooth crossover. When the current quark mass goes to infinity, QCD becomes pure gauge $SU(3)$ theory, and the deconfinement phase transition is of first-order at the critical temperature around $T_c = 270\text{MeV}$. The chiral phase transition mentioned above is crucially dependent on the $U(1)_A$ axial symmetry [42]. For QCD with $N_f = 3$ massless quarks, there is an important QCD phase transition of $U(1)_A$ axial symmetry [43], which is anomalously broken due to quantum effects. This chiral anomaly is closely related to the non-trivial topological QCD theta vacuum structure [44]. The puzzle of the η and η' mass difference or the $U(1)_A$ problem can be resolved by instantons proposed by 't Hooft [45, 46]. The topological structure of QCD vacuum is characterized by an integer-valued Chern-Simons number N_{cs} [47]. Different Chern-Simons sectors are connected through instanton transitions at zero or low temperature and through sphaleron transitions at finite temperature. The change of the Chern-Simons number induces the chirality imbalance between the right-handed and left-handed quarks, which results in a violation of \mathcal{P} - and \mathcal{CP} - symmetry [48–51]. In EW theory, the sphaleron transition is associated with $B + L$ violation, with B the baryon number and L the lepton number [52, 53].

The possibility of local parity violation at high temperatures in high-energy heavy-ion collisions as well as in the early universe was proposed as early as last century [54, 55]. In recent years, QCD phase transition and phase structure under strong magnetic field have attracted much attention, because the magnetic field having a magnitude of 10^{18-20} G (equivalent to $eB \sim (0.1 - 1.0) \text{GeV}^2$) can be generated in non-central heavy-ion collisions [56, 57] at the Relativistic Heavy Ion Collider (RHIC) or the Large Hadron Collider (LHC). It was proposed in Refs. [58–60] that under strong mag-

netic field, a novel phenomenon, the anomalous Chiral Magnetic Effect (CME) can be induced by the chirality imbalance, thus an electromagnetic current can be generated along the magnetic field and the charge separation effect can be induced. The heavy-ion collisions at RHIC and LHC have made great efforts to search the CME through the observation of charge azimuthal correlations [61–63].

The essential ingredient in the CME resulting from the local \mathcal{P} and \mathcal{CP} violation is the chirality imbalance, which is normally introduced by an axial chemical potential μ_5 [58–60]. It is shown in Ref. [64, 65] that the chirality imbalance can be dynamically induced by a repulsive axial vector interaction based on the instanton–anti-instanton ($I\bar{I}$) molecule picture [66–68]. According to Refs. [66–68], the chiral phase transition can be described as a transition from instanton liquid to strongly correlated polarized instanton anti-instanton molecules. Although individual instantons and anti-instantons are strongly suppressed in the chiral symmetric phase, they keep sizable density above T_c and pair up into the ordered instanton anti-instanton molecules when approaching T_c from below. Therefore, the interacting instanton–anti-instanton molecules or pairing can be taken as one possible mechanism describing the nonperturbative effects of QCD in the region of $T \simeq T_c - 2T_c$ [68]. The quark interaction can be induced by the polarized instanton anti-instanton pairing above the critical temperature of the chiral phase transition $T > T_c$, and the corresponding effective Lagrangian density has been derived in Ref. [68] in the form of the four-fermion interactions similar to the Nambu–Jona-Lasinio (NJL) model. Particularly, an unconventional feature was found in Ref. [68] that the iso-scalar axial-vector interaction flips sign and becomes repulsive. This repulsive axial vector interaction spontaneously induces local chirality imbalance and produces a dynamical chiral chemical potential μ_5 in QCD at high temperatures above the chiral phase transition [64, 65]. Also, it is found that the phase transition of the chirality imbalance is of first-order, and increases in magnetic fields help to lower the critical temperature for the appearance of the chirality imbalance. Hence the pairing of the chiral condensate is also affected by the chirality imbalance and is modified by the external magnetic fields at the temperatures around T_c correspondingly. It should be emphasized that the total net topological charge should be zero in the instanton–anti-instanton molecules picture, because the number of instantons is the same as that of anti-instantons. The local chirality imbalance or local \mathcal{P} and \mathcal{CP} violation can be realized with one domain containing more left-handed quarks, while the other domain containing more right-handed quarks.

It is observed in Ref. [65] that the phase transition of the dynamical chirality imbalance with \mathcal{P} and \mathcal{CP} violation is of first-order at high temperature. A first-order phase transition is fascinating in cosmology, possibly resulting in GWs, dark matter, and baryogenesis and thus it would be very interesting to investigate the possible

cosmological signatures of QCD \mathcal{P} and \mathcal{CP} violation. In this work we investigate the GWs spectra and the formation of the primordial black holes related to QCD \mathcal{P} and \mathcal{CP} violation. The primordial black holes (PBHs) have been a source of interest for nearly 50 years and can be generated through multiple approaches, [69–71], among which bubble collision during a first-order phase transition [69, 72, 73], especially a QCD phase transitions [74, 75], is very interesting and has been widely discussed. Strong magnetic field exists in the early universe, though its origin remains a mystery. It was proposed in Ref. [76] that the primordial magnetic fields of order of magnitude of 10^{22} Gauss can be generated in the electroweak scale through chiral anomaly. Therefore, we will also check the effect of the magnetic field on the GWs and PBHs. The paper is organized as following: after Introduction, in Sec. II we introduce the model with spontaneous generation of chirality imbalance induced by a repulsive interaction in the axial vector channel, then in Sec. III, we calculate the α and β parameters to obtain the GWs spectra. In Sec. IV we calculate the possibility of forming primordial black holes. At last, we give summary and conclusion in Sec. V.

II. AXIAL ANOMALY, CHIRALITY IMBALANCE AND FIRST-ORDER PHASE TRANSITION

The nontrivial topological configuration of QCD gauge field is characterized by the integer Chern-Simons number

$$Q_w = \frac{g^2}{32\pi^2} \int d^4x F_{\mu\nu}^a \tilde{F}_a^{\mu\nu} \in \mathbb{Z}, \quad (1)$$

with g the QCD coupling constant, $\text{tr } t_a t_b = \delta_{ab}/2$ the normalized generators, $F_{\mu\nu}^a$ and $\tilde{F}_a^{\mu\nu} = \frac{1}{2}\epsilon_{\mu\nu}^{\rho\sigma} F_{\rho\sigma}^a$ the gluonic field tensor and its dual, respectively. Configurations with nonzero Q_w lead to non-conservation of the axial current even in the chiral limit, which can be seen from the axial Ward-identity:

$$\partial^\mu j_\mu^5 = 2 \sum_f m_f \langle \bar{\psi} i \gamma_5 \psi \rangle_A - \frac{N_f g^2}{16\pi^2} F_{\mu\nu}^a \tilde{F}_a^{\mu\nu}, \quad (2)$$

with N_f the number of quark flavors, ψ a quark field, and m_f the current quark mass, and the axial current has the form of $j_5^\mu = \sum_f \bar{\psi} \gamma^\mu \gamma^5 \psi$. In the chiral limit, we have

$$\partial_\mu j_5^\mu = -\frac{N_f g^2}{16\pi^2} F^{a\mu\nu} \tilde{F}_{\mu\nu}^a. \quad (3)$$

The gauge field configuration with $Q_w \neq 0$ connects different topological vacua characterized by different Chern-Simons numbers, and a positive Q_w convert right-handed fermions into left-handed ones

$$(N_L - N_R)_{t=\infty} = 2N_f Q_w. \quad (4)$$

Therefore, the chirality imbalance is induced by the nonzero topological charge through the axial anomaly of QCD

$$N_5 = \int d^4x \partial_\mu j_5^\mu = -2N_f Q_w, \quad (5)$$

with $N_5 = N_R - N_L$ denoting the number difference between right-handed and left-handed quarks, associated with the isospin singlet axial vector current. Hence, the configuration with nonzero topological charge, depending on the sign of Q_w , can transform left-handed quarks into right-handed or vice versa, and lead to the violation of \mathcal{P} - and \mathcal{CP} - symmetry.

The instanton configuration leads to the famous 't Hooft determinant among quarks with different flavors

$$\mathcal{L}_{t\text{Hooft}} \sim \kappa (\det \bar{\psi}_f P_R \psi_f + \det \bar{\psi}_f P_L \psi_f), \quad (6)$$

which explicitly breaks the $U(1)_A$ symmetry due to the axial anomaly. In Eq. (6) the matrices $P_{R,L} = (1 \pm \gamma_5)/2$ are the chirality projectors. Similarly, the ordered instanton anti-instanton pairing above the chiral critical temperature T_c also results in effective quark interactions, but only in the four-fermion coupling forms. For two-flavor case, above T_c the instanton anti-instanton pairing flips the sign of the axial-vector isoscalar coupling constant from positive to negative [68], therefore one can write the interaction in the following form under magnetic field [64, 65]

$$\mathcal{L} = \bar{\psi} i \gamma_\mu D^\mu \psi + G_S \left[(\bar{\psi} \psi)^2 + (\bar{\psi} i \gamma^5 \tau \psi)^2 \right] - G_V (\bar{\psi} \gamma^\mu \psi)^2 - G_A (\bar{\psi} \gamma^\mu \gamma^5 \psi)^2. \quad (7)$$

Where τ^0 and $\vec{\tau}$ are unit and Pauli matrices in the flavor space respectively, and G_S , G_V and G_A are the coupling constants in the scalar iso-scalar, the vector iso-scalar and the axial-vector isoscalar channels. $D_\mu = \partial_\mu - iq_f A_\mu$ couples quarks with electric charge q_f to a magnetic field $\vec{B} = (0, 0, B)$ with vector potential $A_\mu = (0, 0, -xB, 0)$. The unconventional repulsive axial-vector interaction corresponds to a repulsive axial-vector mean field in the space-like components but an attractive one in the timelike component.

Following Ref. [65], we only keep the scalar iso-scalar and the axial-vector iso-scalar channels that contribute to the phase transition significantly, and rewrite the Lagrangian density under mean field approximation

$$\mathcal{L} = -\frac{\sigma^2}{4G_S} + \frac{\mu_5^2}{4G_A} + \bar{\psi} (i \gamma_\mu D^\mu - \sigma + \mu_5 \gamma^0 \gamma^5) \psi, \quad (8)$$

where $\sigma = -2G_S \langle \bar{\psi} \psi \rangle$ is quark condensate as the order parameter of the chiral phase transition and $\mu_5 = -2G_A \langle \bar{\psi} \gamma^0 \gamma^5 \psi \rangle$ is the dynamical chiral chemical potential describing the chirality imbalance. Then the thermodynamic potential density Ω can be derived and takes

the form of

$$\begin{aligned} \Omega &= \frac{\sigma^2}{4G_S} - \frac{\mu_5^2}{4G_A} \\ &- N_c \sum_{u,d} \frac{|q_f B|}{2\pi} \sum_{s,k} \alpha_{sk} \int_{-\infty}^{+\infty} \frac{dp_z}{2\pi} f_\Lambda^2(p) \omega_{sk}(p) \\ &- 2N_c T \sum_{u,d} \frac{|q_f B|}{2\pi} \sum_{s,k} \alpha_{sk} \int_{-\infty}^{+\infty} \frac{dp_z}{2\pi} \ln(1 + e^{-\beta \omega_{sk}(p)}). \end{aligned} \quad (9)$$

Here $p^2 = p_z^2 + 2|q_f B|k$ with k a natural number marking the Landau levels, and the smooth regularization form factor [77]

$$f_\Lambda(p) = \sqrt{\frac{\Lambda^{10}}{\Lambda^{10} + p^{10}}}, \quad (10)$$

we take $\Lambda = 626.76\text{MeV}$ which satisfies $\Lambda^2 G_S = 2.02$, and use $r_A = \frac{G_A}{G_S}$ to characterize the magnitude of G_A below.

The eigenvalues of the Dirac operator are

$$\omega_{sk} = \sqrt{\sigma^2 + (p + s\mu_5 \text{sgn}(p_z))^2} \quad (11)$$

with $s = \pm 1$, and the spin degeneracy factor is

$$\alpha_{sk} = 1 - \delta_{k,0} + \delta_{k,0} \delta_{s, \text{sgn}(q_f B)}. \quad (12)$$

From Eq. (9), the chiral condensate σ and dynamical chiral chemical potential μ_5 can be determined self-consistently by solving the gap equations

$$\frac{\partial \Omega}{\partial \sigma} = \frac{\partial \Omega}{\partial \mu_5} = 0. \quad (13)$$

The numerical results of chiral condensate σ and dynamical chiral chemical potential μ_5 as a function of the temperature at different eB with varying r_A and at different r_A with varying eB are shown in Fig.1 and Fig. 2, respectively. For every case shown, the thermodynamical potential density always has two or more local minima. For simplicity, we only consider two local minima of each case, one of which indicates non-negative quark condensate σ and zero dynamical chiral chemical potential μ_5 , while the other one is selected from those with positive dynamical chiral chemical potential μ_5 and zero quark condensate σ such that it has the lowest potential density.

From Fig. 1 and Fig. 2, it is observed that the phase transition of the chirality imbalance is always of first-order. The chirality imbalance is induced by the instanton anti-instanton pairing at high temperature, and vanishes at low temperature, which is consistent with the chirality imbalance induced by the exchange of topological Chern-Simons number through instanton transition at low temperature and sphaleron transition at high temperature. At low temperature, the instanton transition rate is exponentially suppressed, while the sphaleron

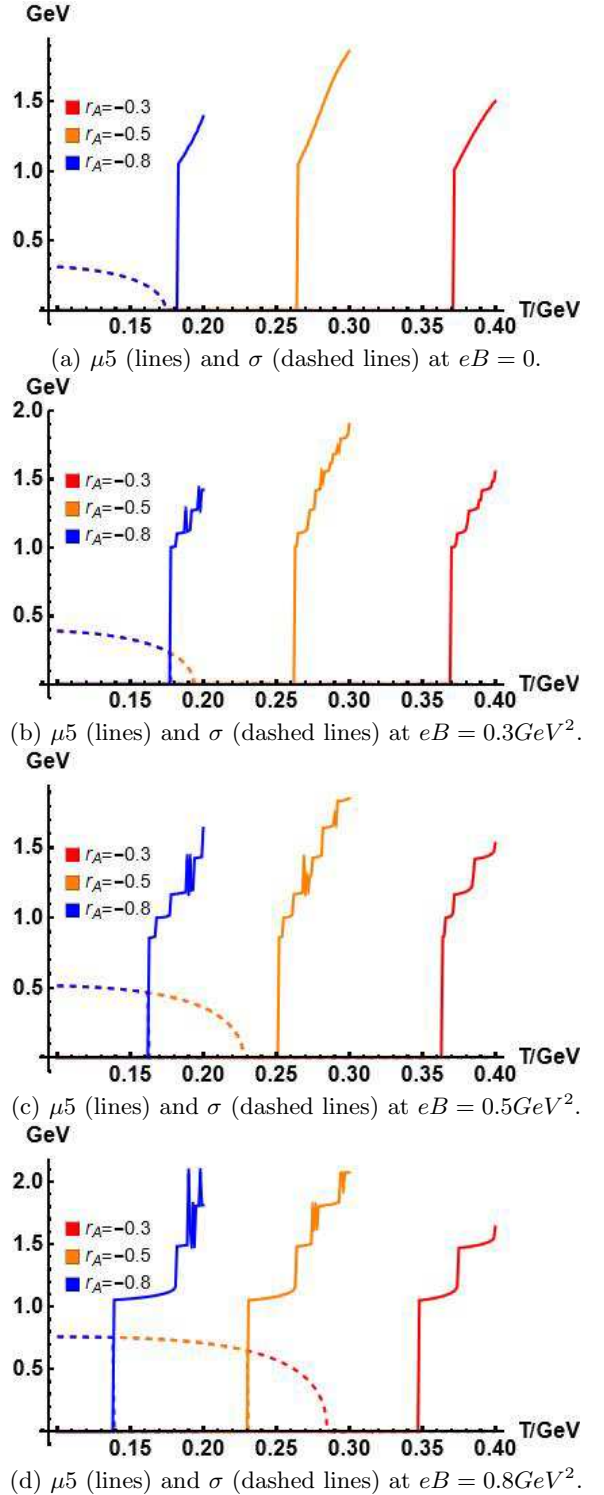


FIG. 1: (Color online) Quark condensate σ (dashed lines) and dynamical chiral chemical potential μ_5 (lines) as a function of T at $eB = 0, 0.3, 0.5$ and 0.8GeV^2 for different values of r_A . σ and μ_5 in unit of GeV.

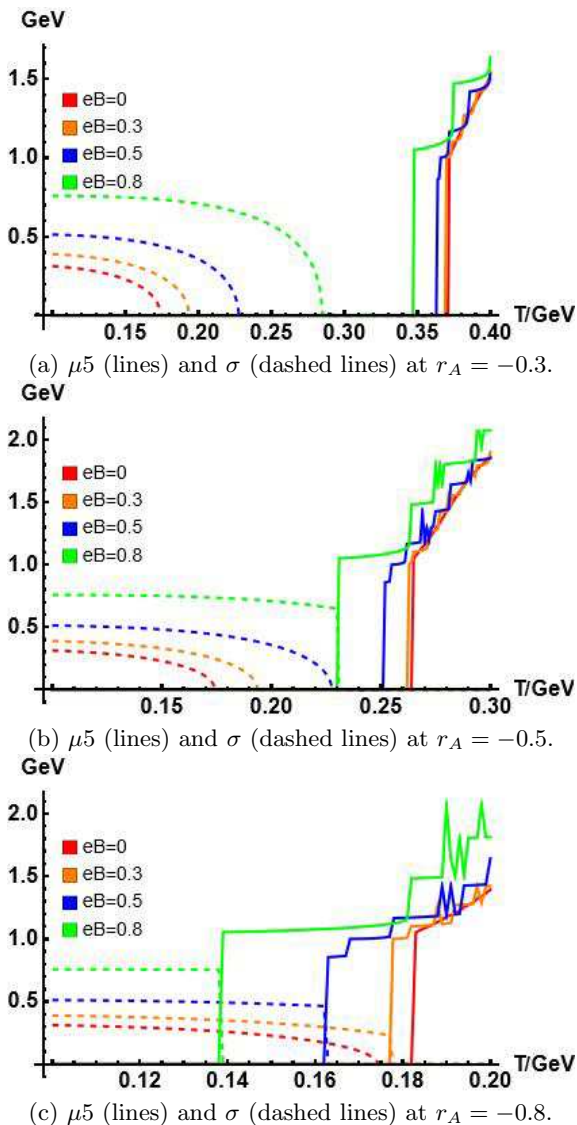


FIG. 2: (Color online) Quark condensate σ (dashed lines) and dynamical chiral chemical potential μ_5 (lines) as a function of T at $r_A = -0.3, -0.5, -0.85$ for different values of eB . σ and μ_5 in unit of GeV, and eB in unit of GeV^2

transition process is enhanced at high temperature because there is sufficient energy to pass over the barrier which separates states of different topological charge.

Fig. 1 shows that the critical temperature of the chirality imbalance $T_c^{\mu_5}$ sensitively drops with stronger axial vector coupling and is not sensitive to the magnetic field. The chiral condensate and corresponding critical temperature T_c^σ are independent of axial vector coupling strength when $T_c^{\mu_5} > T_c^\sigma$. While the magnetic field catalyzes the chiral condensate [78–80] and increases the critical temperature of chiral phase transition T_c^σ . The chiral phase transition is of second-order with small magnitude of magnetic field or/and weak axial vector cou-

pling, and of first-order at strong magnetic field or with strong axial vector coupling. Therefore, one can observe two separated phase transitions with $T_c^{\mu_5} > T_c^\sigma$ with small magnitude of magnetic field or/and with weak axial vector coupling, when the magnitude of the magnetic field or/and the strength of the axial vector coupling increases, these two phase transitions merge into a first-order one with $T_c^{\mu_5} = T_c^\sigma$.

From Fig. 2, we can see how the magnetic field affects the phase transitions more clearly. A magnetic field eB lowers $T_c^{\mu_5}$ but slightly when the axial vector coupling strength is small and raises T_c^σ instead. Namely $T_c^{\mu_5}$ shows an inverse magnetic catalysis effect while both chiral condensate and chiral phase transition show a magnetic catalysis effect. When the axial vector coupling strength grows, we find that the magnetic field has more influences on $T_c^{\mu_5}$ for larger absolute value of r_A , and another interesting result is that when the critical temperature of chiral phase transition T_c^σ meets the one of the phase transition of chirality imbalance $T_c^{\mu_5}$, the chiral phase transition becomes first-order from a second-order one, and if the magnetic field continue to grow, the catalysis effect of magnetic field on chiral phase transition is blunted or even inverse [81–83]. This is the main result in Ref. [65] to explain the inverse magnetic catalysis, while in this work, we are interested in the first-order phase transition of the chirality imbalance. In the following, we will investigate the GWs spectra and the generation of the PBHs from this phase transition.

III. GRAVITATIONAL WAVES

In the previous section we find that the phase transition of the chirality imbalance is always a first order one at high temperature. Once the phase transition starts, part of the universe tunnels to the true vacuum, forming bubbles with lower vacuum energy density, then the latent heat released is converted into the energy of the bubble walls. These bubbles expand and collide and pass kinetic energy to surrounding media, generating GWs from the scalar field, the sound waves and the magnetohydrodynamic (MHD) turbulence.

To obtain the spectra of GWs, we assume that the velocity of the bubble walls is $v_w = 0.99$ and thus the scalar field contribution is negligibly small. Only the GWs from the latter two sources contribute to the total energy density spectrum [84], i.e.

$$h^2\Omega = h^2\Omega_{sw} + h^2\Omega_{tb}. \quad (14)$$

The bubble nucleation rate per Hubble volume per time is [85–87]

$$\Gamma(t) = Ae^{S_4(t)}, \quad (15)$$

where S_4 is Euclidean action of an O_4 -symmetric solution and reduces to $\frac{S_3}{T}$ at finite temperature T . And the

coefficient A is [88]

$$A(T) = T^4 \left(\frac{S_3}{2\pi T} \right)^{\frac{3}{2}}. \quad (16)$$

Bubbles of true vacuum start to occur when the universe cools down to the nucleation temperature T_n , at which we have [86, 87]

$$\Gamma(t)H_*^4 \sim 1, \quad (17)$$

where H_* is the corresponding Hubble parameter. Approximately T_n is also the temperature of the thermal bath with weak reheating, thus we have

$$\frac{\beta}{H_*} = T_n \left. \frac{d(\frac{S_3}{T})}{dT} \right|_{T_n}, \quad (18)$$

where parameter β measures the transition rate.

For our model, $g_* = 12$ is the number of relativistic degrees of freedom, and hence the energy density of the radiation bath is $\rho_r = \frac{\pi^2 g_* T^4}{30}$. With the energy density difference between the false vacuum and the true vacuum ρ_{vac} , another parameter that measures the transition strength can be written as [86, 88]

$$\begin{aligned} \alpha &= \frac{1}{\rho_r} \left(\rho_{vac} - \frac{T}{4} \left. \frac{\partial \rho_{vac}}{\partial T} \right|_{T_p} \right) \\ &\approx \frac{1}{\rho_r} \left(\rho_{vac} - \frac{T}{4} \left. \frac{\partial \rho_{vac}}{\partial T} \right|_{T_n} \right), \end{aligned} \quad (19)$$

where T_p is the percolation temperature. As shown below, $\frac{\beta}{H_*}$ is so large that the false vacuum decays rapidly, hence the temperature is nearly constant during the phase transition, then we have $T_p \approx T_n$.

In addition, the Friedmann equation is

$$H_* = \sqrt{\frac{\rho_r + \rho_{vac}}{3m_p^2}} \quad (20)$$

with the reduced Planck Mass $m_p = 2.435 \times 10^{18} GeV$.

Meanwhile, parameters κ_v and κ_{tb} are respectively the fraction of the false vacuum energy converted into the kinetic energy of the plasma and the MHD turbulence which can be analytically fitted [84, 89, 90]

$$\kappa_v (v_w \sim 1) = \alpha (0.73 + 0.083\sqrt{\alpha} + \alpha)^{-1}. \quad (21)$$

Simulations give $\frac{\kappa_{tb}}{\kappa_v} \sim 0.05 - 0.1$ [84, 91] and here we take $\kappa_{tb} = 0.05\kappa_v$.

In terms of the parameters above, the numerical results of GWs from sound waves and MHD turbulence are respectively [84, 88]

$$h^2 \Omega_{sw}(f) = 2.65 \times 10^{-6} \left(\frac{H_*}{\beta} \right) \left(\frac{\kappa_v \alpha}{1 + \alpha} \right)^2 \left(\frac{100}{g_*} \right)^{\frac{1}{3}} v_w S_{sw}(f) \quad (22)$$

and

$$h^2 \Omega_{tb}(f) = 3.35 \times 10^{-4} \left(\frac{H_*}{\beta} \right) \left(\frac{\kappa_{tb} \alpha}{1 + \alpha} \right)^2 \left(\frac{100}{g_*} \right)^{\frac{1}{3}} v_w S_{tb}(f), \quad (23)$$

where

$$S_{sw}(f) = \left(\frac{f}{f_{sw}} \right)^3 \left(\frac{7}{4 + 3 \left(\frac{f}{f_{sw}} \right)^2} \right)^{\frac{7}{2}}, \quad (24)$$

$$S_{tb}(f) = \left(\frac{f}{f_{tb}} \right)^3 \left(1 + \frac{f}{f_{tb}} \right)^{-\frac{11}{3}} \left(1 + \frac{8\pi f}{h_*} \right)^{-1}. \quad (25)$$

The peak frequencies of the two sources are

$$f_{sw} = 1.9 \times 10^{-5} \frac{1}{v_w} \frac{\beta}{H_*} \frac{T_n}{100 GeV} \left(\frac{g_*}{100} \right)^{\frac{1}{6}} Hz \quad (26)$$

and

$$f_{tb} = 2.7 \times 10^{-5} \frac{1}{v_w} \frac{\beta}{H_*} \frac{T_n}{100 GeV} \left(\frac{g_*}{100} \right)^{\frac{1}{6}} Hz. \quad (27)$$

$$h_* = 1.65 \times 10^{-6} \frac{T_n}{100 GeV} \left(\frac{g_*}{100} \right)^{\frac{1}{6}} Hz \quad (28)$$

is the Hubble rate.

B/GeV^2	r_A	T_n/GeV	α	β/H_*
0	-0.3	0.3648	0.7343	27582
0	-0.5	0.2561	1.741	16274
0	-0.8	0.1679	4.850	6105.7
0.3	-0.3	0.3634	0.7727	30478
0.3	-0.5	0.2535	1.790	14660
0.3	-0.8	0.1635	5.375	12028
0.5	-0.3	0.3517	0.7384	22859
0.5	-0.5	0.2393	1.745	11136
0.5	-0.8	0.1389	8.364	2579.0
0.8	-0.3	0.3402	1.166	25235
0.8	-0.5	0.2126	2.633	11171
0.8	-0.8	0.1079	28.67	2819.5

TABLE I: Nucleation temperature T_n , parameters α and β corresponding to different values of r_A and eB .

Table I lists nucleation temperature T_n and key parameters α and $\frac{\beta}{H_*}$ corresponding to different values of r_A and eB . Larger eB or/and larger magnitude of r_A brings lower nucleation temperature T_n and thus lower peak frequencies without peaks raised according to Eq. (26) and Eq. (27). Larger magnitude of r_A also brings smaller $\frac{\beta}{H_*}$ and larger α while values of eB have slight influence on these two parameters, and further smaller values of $\frac{\beta}{H_*}$ raise peaks according to Eq. (22) and Eq.

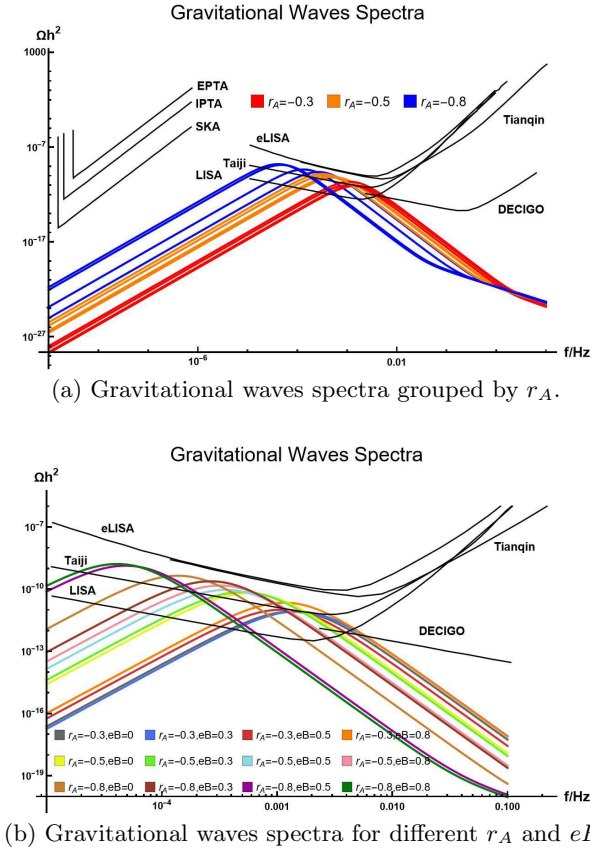


FIG. 3: (Color online) Gravitational waves spectra for $r_A = -0.3, -0.5, -0.8$ with different values of $eB = 0, 0.3, 0.5, 0.8 \text{ GeV}^2$.

(23) and lower peak frequencies according to Eq. (26) and Eq. (27), simultaneously. Additionally, α has no significant influence on spectra.

Fig. 3 shows spectra of GWs with different values of parameters r_A and eB . Fig. 3 a) shows groups of spectra for $r_A = -0.3, -0.5, -0.8$ and detailed curves for different eB can be found in Fig. 3 b). In Fig. 3 a), the peak frequencies are in the range of about 10^{-5} Hz to 10^{-2} Hz, starting around 0.001 Hz for $r_A = -0.3$ and shifting to lower values with increases in the strength of r_A . The energy density peaks start from around 10^{-11} for $r_A = -0.3$ and rise to 10^{-9} for $r_A = -0.8$.

Fig. 3 b) shows the details for different values of r_A and eB , where we can read the effect of the magnetic field. In general, weaker magnetic field gives higher peak frequency and lower energy density peak, with the increase in the magnetic field, the peak frequency decreases and peak energy density rises. Increasing magnitudes of both r_A and eB enhance the peak energy density, and the peak energy density reaches the highest in the case of $r_A = -0.8, eB = 0.8$.

With the parameters we consider, the GWs produced by chirality imbalance are detectable for LISA, Taiji and DECIGO [92, 93], but too weak to be detectable for

eLISA and Tianqin. The spectrum with larger magnitude of r_A has higher peak energy density and lower peak frequency. According to this trend, if the magnitude of r_A is large enough the spectrum may be able to be detected by SKA, IPTA and EPTA, while the spectrum falls to zero finally with vanishing r_A , meaning no first-order phase transition can be induced when the axial vector coupling constant is non-negative (see Ref. [65]).

IV. PRIMORDIAL BLACK HOLES

Ref. [94] proposes a mechanism for PBHs formation during a first-order phase transition. There probably are some areas in the universe in which the false vacuum defers decay and the postponement of decay can lead to primordial black holes. Outside such areas the phase transition starts when $\Gamma(t)H_*^4 \sim 1$ and the false vacuum energy density released is converted into other types of energy density, e.g. the radiation energy density ρ_r , which decays during the expansion of the universe $\rho_r \propto a^{-4}$. While inside these areas the phase transition is delayed for a certain time and the false vacuum energy density ρ_{vac} stored does not decay during the expansion. Thus the energy density is larger inside than outside when the phase transition completes. If the contrast of the energy density reaches the threshold $\delta_c + 1 = 1.41$ [95], these over-dense areas can collapse into PBHs. In this section, following Ref. [94], we set $8\pi G = 1$.

The bubble nucleation rate per Hubble volume per time can be expanded as [85, 86]

$$\Gamma(t) = \Gamma_0 e^{\beta t}, \quad (29)$$

then the volume fraction of the remaining false vacuum is [96]

$$F(t) = \exp\left(-\frac{4\pi}{3} \int_{t_i}^t dt' \Gamma(t') R^3(t') r^3(t, t')\right), \quad (30)$$

where $r(t, t') = \int_{t'}^t dt'' \frac{v_w(t'')}{R(t'')}$ is the comoving radius of a bubble which was nucleated at time t' . Therefore the false vacuum energy density can be written as

$$\rho_v(t) = \rho_{vac} F(t). \quad (31)$$

Typically, we choose $\frac{\beta}{H} = 16274$ and $\alpha = 1.741$. Without significant reheating, we approximately have $\alpha = \frac{\rho_{vac}}{\rho_r(t)}$ [84].

With the energy density of the bubble walls ρ_w , the Friedmann equation is now

$$H = \sqrt{\frac{\rho_v + \rho_r + \rho_w}{3}}. \quad (32)$$

Then the evolution of energy density satisfies

$$\frac{d(\rho_r + \rho_w)}{dt} + 4H(\rho_r + \rho_w) = -\frac{d\rho_v}{dt}. \quad (33)$$

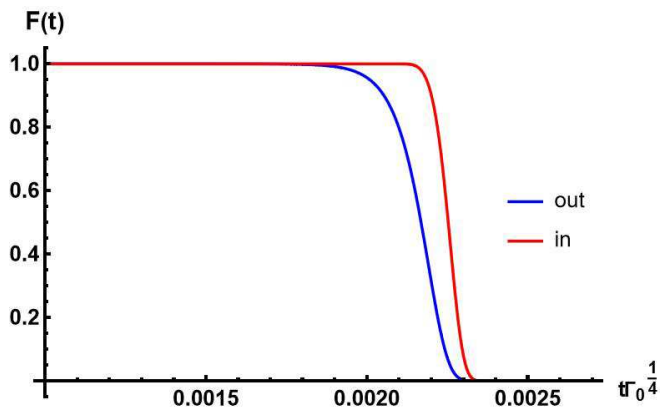


FIG. 4: The evolution of the fraction of the false vacuum.

Fig. 4 shows the evolution of the volume fraction of the false vacuum. $F(t)$ falls sharply from 1 to near 0 in a very short time, thus the phase transition progresses rapidly and we can assume the bubble nucleation rate $\Gamma_0 H_*^4 = 1$ at the initial time $t_i = 0$. The time when the first bubble occurs inside over-dense areas is approximately set $t_n \Gamma_0^{\frac{1}{4}} = 0.0021$ when $F(t)$ outside is around 0.7. Since the duration of the phase transition is short in the expanding universe, H_* is approximately invariant for simplicity when calculating Eq. (29) and Eq. (30). Combining and solving Eq. (31), Eq. (32) and Eq. (33), we can then numerically calculate the evolution of the energy density inside and outside the over-dense areas.

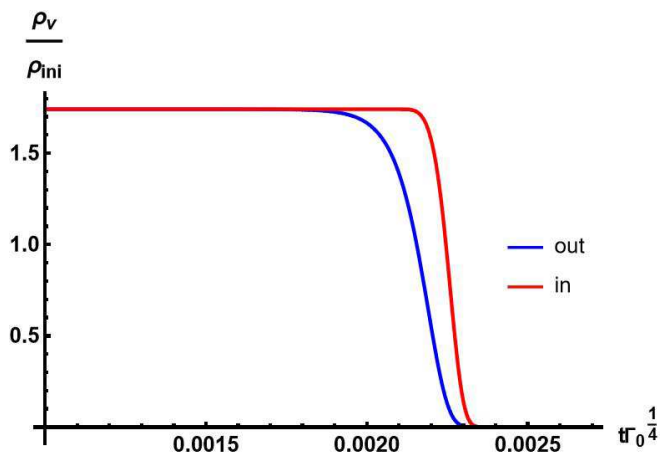


FIG. 5: The evolution of the energy density of the false vacuum inside and outside the over-dense area.

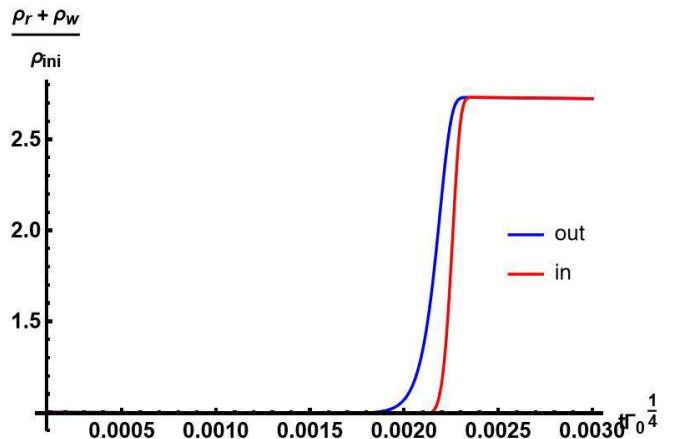


FIG. 6: The evolution of the energy density of the radiation and bubble walls inside and outside the over-dense area.

Fig. 5 and Fig. 6 show the inside and outside evolution of the energy density scaled by ρ_{ini} , the initial value of ρ_r . However, in our model the false vacuum sharply decays to the true vacuum, the decay in over-dense areas cannot be postponed long enough for the energy density contrast to reach the threshold. As shown in Fig. 6, the terminal energy density inside the over-dense region is indeed but very slightly larger than outside, therefore given that threshold δ_c it is hardly possible to form primordial black holes through postponement of the phase transition induced by chirality imbalance without significant supercooling. If we set larger $t_n \Gamma_0^{\frac{1}{4}}$, the contrast of the energy density increases slightly but the corresponding possibility drops.

V. SUMMARY AND DISCUSSION

The nonperturbative topological structure of QCD vacuum is an important feature of pure gauge field theory, which attracts wide interest not only in the little bang in heavy-ion collisions, but also in the big bang in early universe. The topological structure of QCD vacuum characterized by integer-valued Chern-Simons number, and the change of the Chern-Simons number induces the chirality imbalance between the right-handed and left-handed number of quarks through instanton transitions at zero or low temperatures and through sphaleron transitions at high temperatures, which results in a violation of \mathcal{P} - and \mathcal{CP} - symmetry. The instanton transition rate is exponentially suppressed at low temperature, while the sphaleron transition process is enhanced at high temperature. The chirality imbalanced QCD matter with local \mathcal{P} and \mathcal{CP} violation related to the observation of CME in heavy-ion collisions could shed light on the mechanism of baryon asymmetry generation in the early universe [97]. In this work, we take a model with repulsive interaction in the axial vector channel derived from the instanton

anti-instanton pairing, and the chirality imbalance can be spontaneously induced at high temperature above the chiral phase transition, and vanishes at low temperature. We investigate the cosmological observations related to QCD phase transition with \mathcal{P} and \mathcal{CP} violation.

It is found that the phase transition of the chirality imbalance is always a first-order phase transition, and the critical temperature of the chirality imbalance $T_c^{\mu_5}$ is sensitively lowered by larger magnitude of the axial vector coupling constant but not much by stronger magnetic field. The chiral phase transition is of second-order with weak magnetic field and small magnitude of the axial vector coupling constant and in this situation the chiral condensate is catalyzed by the magnetic field with corresponding critical temperature T_c^σ raised but independent of the axial vector coupling constant. It becomes first-order with strong magnetic field and large magnitude of axial vector coupling constant and in this situation, if the magnetic field continue to grow, the chiral condensate is less or inversely catalyzed with decreasing critical temperature keeping $T_c^\sigma = T_c^\mu$. Therefore, two phase transitions are separated when $T_c^{\mu_5} > T_c^\sigma$, when the magnitudes of the magnetic field and axial vector coupling constant are large enough, the chiral phase transition becomes first-order with $T_c^{\mu_5} = T_c^\sigma$ so that these two phase transitions merge into a first-order one and the magnetic catalysis effect is blunted or inverse.

Then we investigate the generation of GWs from this first-order phase transition and consider the effect of a strong magnetic field. We calculate the corresponding parameters α and β for different values of parameters r_A and eB and obtain the GWs spectra. We select two figures of spectra to demonstrate changes of spectra with r_A or eB . Weaker magnetic field gives higher peak frequency and lower peak energy density, with the increase in the magnetic field, the peak frequency decreases and peak energy density rises. Increasing magnitudes of both r_A and eB enhance the peak energy density, and the peak energy density reaches the highest in the case of $r_A = -0.8, eB = 0.8$. The GWs spectra produced by chirality imbalance are detectable for LISA, Taiji and DECIGO, with the peak energy density locating in the range of $10^{-11} - 10^{-9}$, and the peak frequency lying in the range of 10^{-5} Hz to 10^{-2} Hz. The spectrum with larger magnitude of axial vector coupling constant and stronger magnetic field has higher peak energy density and lower peak frequency. According to this trend, the GWs spectra might also be able to be detected by SKA, IPTA and EPTA.

At last, we investigate the possibility of formation of the PBHs from this first-order phase transition based on the mechanism of postponement of false vacuum decay. We calculate the evolution of the energy density inside

and outside those over-dense areas, and find that with typical parameters the phase transition completes in a too short time and thus the false vacuum energy density decays sharply. The postponement cannot last long while keeping feasible possibility, hence the contrast of the energy density inside and outside over-dense areas can hardly reach the threshold 1.41 and it is scarcely possible to form PBHs in our model.

With typical parameters above, the phase transition induces GWs that can only be detected by LISA, Taiji and DECIGO. However, if the phase transition occurs with much stronger supercooling, the situation becomes different and intriguing. Lower transition temperature means larger α and much smaller $\frac{\beta}{H_*}$. With strong supercooling alone, e.g. we have $\frac{\beta}{H_*} \sim 10$, the peak of the spectrum moves to the upper left and thus the GWs can also be detected by SKA, IPTA and EPTA with peak frequencies $f \sim 10^{-7}$ Hz and peak energy density around 10^{-7} . If a weaker supercooling happens (e.g. we have $\frac{\beta}{H_*} \sim 1000$) and simultaneously T_n is higher when we have tiny magnitude of r_A , the peak then rises and the GWs are detectable for Tianqin and eLISA.

Furthermore, if we have $\frac{\beta}{H_*} \sim 1$, the decay of the false vacuum can be postponed longer enough (e.g. $t_n \Gamma_0^{\frac{1}{4}} \sim 1$), so that the contrast of the energy density inside and outside can probably reach the threshold, thus it is possible to form PBHs. Since strong supercooling demands some part of the universe remains the false vacuum in spite of the nucleation rate $\Gamma(t)H_*^4 \gg 1$, the possibility of such situation is extremely slight. Though postponement of the false vacuum decay has negligible possibility to form PBHs in this model, other mechanisms may work, e.g. bubble collisions [98, 99], density fluctuations [100]. Meanwhile, if there exist a dust-like phase which lowers acoustic speed c_s during a QCD phase transition, the threshold δ_c decreases and make it easier to form PBHs [101, 102].

ACKNOWLEDGMENTS

We thank Yidian Chen, Huaike Guo, Mingqiu Li, Jing Liu and Qishu Yan for helpful discussions. This work is supported in part by the National Natural Science Foundation of China (NSFC) Grant Nos. 12235016, 12221005, 11725523 and 11735007, the Strategic Priority Research Program of Chinese Academy of Sciences under Grant Nos XDB34030000 and XDPB15, the start-up funding from University of Chinese Academy of Sciences (UCAS), and the Fundamental Research Funds for the Central Universities.

[1] Albert Einstein. Approximative Integration of the Field Equations of Gravitation. *Sitzungsber. Preuss. Akad.*

Wiss. Berlin (Math. Phys.), 1916:688–696, 1916.

- [2] Albert Einstein. Über Gravitationswellen. *Sitzungsber. Preuss. Akad. Wiss. Berlin (Math. Phys.)*, 1918:154–167, 1918.
- [3] B. P. Abbott et al. Observation of Gravitational Waves from a Binary Black Hole Merger. *Phys. Rev. Lett.*, 116(6):061102, 2016.
- [4] B. P. Abbott et al. GW170817: Observation of Gravitational Waves from a Binary Neutron Star Inspiral. *Phys. Rev. Lett.*, 119(16):161101, 2017.
- [5] Michele Maggiore. Gravitational wave experiments and early universe cosmology. *Physics Reports*, 331(6):283–367, 2000.
- [6] Keith Riles. Gravitational waves: Sources, detectors and searches. *Progress in Particle and Nuclear Physics*, 68:1–54, 2013.
- [7] M. Punturo et al. The Einstein Telescope: A third-generation gravitational wave observatory. *Class. Quant. Grav.*, 27:194002, 2010.
- [8] Mark Hannam and Ian Hawke. Numerical relativity simulations in the era of the einstein telescope. *General Relativity and Gravitation*, 43(2):465–483, 2011.
- [9] Peter W. Graham, Jason M. Hogan, Mark A. Kasevich, Surjeet Rajendran, and Roger W. Romani. Mid-band gravitational wave detection with precision atomic sensors. 11 2017.
- [10] L. Badurina et al. AION: An Atom Interferometer Observatory and Network. *JCAP*, 05:011, 2020.
- [11] Yousef Abou El-Neaj et al. AEDGE: Atomic Experiment for Dark Matter and Gravity Exploration in Space. *EPJ Quant. Technol.*, 7:6, 2020.
- [12] C. Cutler and J. Harms. BBO and the neutron-star-binary subtraction problem. *Phys. Rev. D*, 73:042001, 2006.
- [13] Seiji Kawamura et al. The Japanese space gravitational wave antenna: DECIGO. *Class. Quant. Grav.*, 28:094011, 2011.
- [14] Shuichi Sato et al. The status of DECIGO. *J. Phys. Conf. Ser.*, 840(1):012010, 2017.
- [15] Pau Amaro-Seoane et al. Laser Interferometer Space Antenna. 2 2017.
- [16] Wen-Rui Hu and Yue-Liang Wu. The Taiji Program in Space for gravitational wave physics and the nature of gravity. *Natl. Sci. Rev.*, 4(5):685–686, 2017.
- [17] Wen-Hong Ruan, Zong-Kuan Guo, Rong-Gen Cai, and Yuan-Zhong Zhang. Taiji program: Gravitational-wave sources. *Int. J. Mod. Phys. A*, 35(17):2050075, 2020.
- [18] Jun Luo et al. TianQin: a space-borne gravitational wave detector. *Class. Quant. Grav.*, 33(3):035010, 2016.
- [19] Stephen R Taylor. The nanohertz gravitational wave astronomer. *arXiv preprint arXiv:2105.13270*, 2021.
- [20] RW Hellings and GS Downs. Upper limits on the isotropic gravitational radiation background from pulsar timing analysis. *The Astrophysical Journal*, 265:L39–L42, 1983.
- [21] Zaven Arzoumanian, Paul T Baker, Harsha Blumer, Bence Bécsy, Adam Brazier, Paul R Brook, Sarah Burke-Spolaor, Shami Chatterjee, Siyuan Chen, James M Cordes, et al. The nanograv 12.5 yr data set: search for an isotropic stochastic gravitational-wave background. *The Astrophysical journal letters*, 905(2):L34, 2020.
- [22] B B P Perera, M E DeCesar, P B Demorest, M Kerr, L Lentati, D J Nice, S Osłowski, S M Ransom, M J Keith, Z Arzoumanian, M Bailes, P T Baker, C G Bassa, N D R Bhat, A Brazier, M Burgay, S Burke-Spolaor, R N Caballero, D J Champion, S Chatterjee, S Chen, I Cognard, J M Cordes, K Crowter, S Dai, G Desvignes, T Dolch, R D Ferdman, E C Ferrara, E Fonseca, J M Goldstein, E Graikou, L Guillemot, J S Hazboun, G Hobbs, H Hu, K Islo, G H Janssen, R Karuppusamy, M Kramer, M T Lam, K J Lee, K Liu, J Luo, A G Lyne, R N Manchester, J W McKee, M A McLaughlin, C M F Mingarelli, A P Parthasarathy, T T Pennucci, D Perrodin, A Possenti, D J Reardon, C J Russell, S A Sanidas, A Sesana, G Shaifullah, R M Shannon, X Siemens, J Simon, R Spiewak, I H Stairs, B W Stappers, J K Swiggum, S R Taylor, G Theureau, C Tiburzi, M Vallisneri, A Vecchio, J B Wang, S B Zhang, L Zhang, W W Zhu, and X J Zhu. The International Pulsar Timing Array: second data release. *Monthly Notices of the Royal Astronomical Society*, 490(4):4666–4687, 10 2019.
- [23] G. Desvignes, R. N. Caballero, L. Lentati, J. P. W. Verbiest, D. J. Champion, B. W. Stappers, G. H. Janssen, P. Lazarus, S. Osłowski, S. Babak, C. G. Bassa, P. Brem, M. Burgay, I. Cognard, J. R. Gair, E. Graikou, L. Guillemot, J. W. T. Hessels, A. Jessner, C. Jordan, R. Karuppusamy, M. Kramer, A. Lassus, K. Lazaridis, K. J. Lee, K. Liu, A. G. Lyne, J. McKee, C. M. F. Mingarelli, D. Perrodin, A. Petiteau, A. Possenti, M. B. Purver, P. A. Rosado, S. Sanidas, A. Sesana, G. Shaifullah, R. Smits, S. R. Taylor, G. Theureau, C. Tiburzi, R. van Haasteren, and A. Vecchio. High-precision timing of 42 millisecond pulsars with the European Pulsar Timing Array. *Monthly Notices of the Royal Astronomical Society*, 458(3):3341–3380, 03 2016.
- [24] Richard T. Schilizzi, Peter E. F. Dewdney, and T. Joseph W. Lazio. The square kilometre array. In Larry M. Stepp, Roberto Gilmozzi, and Helen J. Hall, editors, *Ground-based and Airborne Telescopes III*, volume 7733, page 773318. International Society for Optics and Photonics, SPIE, 2010.
- [25] Amanda Weltman, P Bull, S Camera, K Kelley, H Padmanabhan, J Pritchard, A Raccanelli, S Riemer-Sørensen, L Shao, S Andrianomena, et al. Fundamental physics with the square kilometre array. *Publications of the Astronomical Society of Australia*, 37, 2020.
- [26] Rendong Nan, Di Li, Chengjin Jin, Qiming Wang, Lichun Zhu, Wenbai Zhu, Haiyan Zhang, Youling Yue, and Lei Qian. The Five-Hundred-Meter Aperture Spherical Radio Telescope (FAST) Project. *Int. J. Mod. Phys. D*, 20:989–1024, 2011.
- [27] Marc Kamionkowski, Arthur Kosowsky, and Albert Stebbins. A probe of primordial gravity waves and vorticity. *Physical Review Letters*, 78(11):2058, 1997.
- [28] Hong Li et al. Probing Primordial Gravitational Waves: Ali CMB Polarization Telescope. *Natl. Sci. Rev.*, 6(1):145–154, 2019.
- [29] Nancy Aggarwal et al. Challenges and opportunities of gravitational-wave searches at MHz to GHz frequencies. *Living Rev. Rel.*, 24(1):4, 2021.
- [30] Aaron S Chou, Richard Gustafson, Craig Hogan, Brittany Kamai, Ohkyung Kwon, Robert Lanza, Shane L Larson, Lee McCuller, Stephan S Meyer, Jonathan Richardson, et al. Mhz gravitational wave constraints with decameter michelson interferometers. *Physical Review D*, 95(6):063002, 2017.
- [31] C. J. Moore, R. H. Cole, and C. P. L. Berry. Gravitational-wave sensitivity curves. *Class. Quant.*

- Grav.*, 32(1):015014, 2015.
- [32] Odylio Denys Aguiar. The Past, Present and Future of the Resonant-Mass Gravitational Wave Detectors. *Res. Astron. Astrophys.*, 11:1–42, 2011.
- [33] C. J. Hogan. Gravitational radiation from cosmological phase transitions. *Mon. Not. Roy. Astron. Soc.*, 218:629–636, 1986.
- [34] Arthur Kosowsky, Michael S. Turner, and Richard Watkins. Gravitational waves from first order cosmological phase transitions. *Phys. Rev. Lett.*, 69:2026–2029, 1992.
- [35] Arthur Kosowsky and Michael S. Turner. Gravitational radiation from colliding vacuum bubbles: envelope approximation to many bubble collisions. *Phys. Rev. D*, 47:4372–4391, 1993.
- [36] Marc Kamionkowski, Arthur Kosowsky, and Michael S. Turner. Gravitational radiation from first order phase transitions. *Phys. Rev. D*, 49:2837–2851, 1994.
- [37] Stefano Profumo, Michael J. Ramsey-Musolf, and Gabe Shaughnessy. Singlet Higgs phenomenology and the electroweak phase transition. *JHEP*, 08:010, 2007.
- [38] P. H. Damgaard, A. Haarr, D. O’Connell, and A. Tranberg. Effective Field Theory and Electroweak Baryogenesis in the Singlet-Extended Standard Model. *JHEP*, 02:107, 2016.
- [39] Ville Vaskonen. Electroweak baryogenesis and gravitational waves from a real scalar singlet. *Phys. Rev. D*, 95(12):123515, 2017.
- [40] F. Karsch. Lattice QCD at high temperature and density. *Lect. Notes Phys.*, 583:209–249, 2002.
- [41] Y. Aoki, G. Endrodi, Z. Fodor, S. D. Katz, and K. K. Szabo. The Order of the quantum chromodynamics transition predicted by the standard model of particle physics. *Nature*, 443:675–678, 2006.
- [42] Robert D. Pisarski and Frank Wilczek. Remarks on the Chiral Phase Transition in Chromodynamics. *Phys. Rev. D*, 29:338–341, 1984.
- [43] H. T. Ding, S. T. Li, Swagato Mukherjee, A. Tomiya, X. D. Wang, and Y. Zhang. Correlated Dirac Eigenvalues and Axial Anomaly in Chiral Symmetric QCD. *Phys. Rev. Lett.*, 126(8):082001, 2021.
- [44] Mark Srednicki. Axions: Past, present, and future. In *Continuous Advances in QCD 2002 / ARKADYFEST (honoring the 60th birthday of Prof. Arkady Vainshtein)*, pages 509–520, 10 2002.
- [45] Gerard ’t Hooft. Symmetry Breaking Through Bell-Jackiw Anomalies. *Phys. Rev. Lett.*, 37:8–11, 1976.
- [46] Gerard ’t Hooft. How Instantons Solve the U(1) Problem. *Phys. Rept.*, 142:357–387, 1986.
- [47] A. A. Belavin, Alexander M. Polyakov, A. S. Schwartz, and Yu. S. Tyupkin. Pseudoparticle Solutions of the Yang-Mills Equations. *Phys. Lett. B*, 59:85–87, 1975.
- [48] Edward Witten. Current Algebra Theorems for the U(1) Goldstone Boson. *Nucl. Phys. B*, 156:269–283, 1979.
- [49] G. Veneziano. U(1) Without Instantons. *Nucl. Phys. B*, 159:213–224, 1979.
- [50] Ettore Vicari and Haralambos Panagopoulos. Theta dependence of SU(N) gauge theories in the presence of a topological term. *Phys. Rept.*, 470:93–150, 2009.
- [51] Thomas Schäfer and Edward V. Shuryak. Instantons in QCD. *Rev. Mod. Phys.*, 70:323–426, 1998.
- [52] V. A. Kuzmin, V. A. Rubakov, and M. E. Shaposhnikov. On the Anomalous Electroweak Baryon Number Nonconservation in the Early Universe. *Phys. Lett. B*, 155:36, 1985.
- [53] M. E. Shaposhnikov. Baryon Asymmetry of the Universe in Standard Electroweak Theory. *Nucl. Phys. B*, 287:757–775, 1987.
- [54] P. D. Morley and I. A. Schmidt. Strong P, CP, T Violations in Heavy Ion Collisions. *Z. Phys. C*, 26:627, 1985.
- [55] Dmitri Kharzeev, R. D. Pisarski, and Michel H. G. Tytgat. Possibility of spontaneous parity violation in hot QCD. *Phys. Rev. Lett.*, 81:512–515, 1998.
- [56] V. Skokov, A. Yu. Illarionov, and V. Toneev. Estimate of the magnetic field strength in heavy-ion collisions. *Int. J. Mod. Phys. A*, 24:5925–5932, 2009.
- [57] Wei-Tian Deng and Xu-Guang Huang. Event-by-event generation of electromagnetic fields in heavy-ion collisions. *Phys. Rev. C*, 85:044907, 2012.
- [58] D. Kharzeev and A. Zhitnitsky. Charge separation induced by P-odd bubbles in QCD matter. *Nucl. Phys. A*, 797:67–79, 2007.
- [59] Dmitri E. Kharzeev, Larry D. McLerran, and Harmen J. Warringa. The Effects of topological charge change in heavy ion collisions: ‘Event by event P and CP violation’. *Nucl. Phys. A*, 803:227–253, 2008.
- [60] Kenji Fukushima, Dmitri E. Kharzeev, and Harmen J. Warringa. The Chiral Magnetic Effect. *Phys. Rev. D*, 78:074033, 2008.
- [61] B. I. Abelev et al. Observation of charge-dependent azimuthal correlations and possible local strong parity violation in heavy ion collisions. *Phys. Rev. C*, 81:054908, 2010.
- [62] Betty Abelev et al. Charge separation relative to the reaction plane in Pb-Pb collisions at $\sqrt{s_{NN}} = 2.76$ TeV. *Phys. Rev. Lett.*, 110(1):012301, 2013.
- [63] Search for the Chiral Magnetic Effect in Au+Au collisions at $\sqrt{s_{NN}} = 27$ GeV with the STAR forward Event Plane Detectors. 9 2022.
- [64] Zhao Zhang. Correction to the Chiral Magnetic Effect from axial-vector interaction. *Phys. Rev. D*, 85:114028, 2012.
- [65] Lang Yu, Hao Liu, and Mei Huang. Spontaneous generation of local CP violation and inverse magnetic catalysis. *Phys. Rev. D*, 90(7):074009, 2014.
- [66] Ernst-Michael Ilgenfritz and Edward V. Shuryak. Chiral Symmetry Restoration at Finite Temperature in the Instanton Liquid. *Nucl. Phys. B*, 319:511–520, 1989.
- [67] Ernst-Michael Ilgenfritz and Edward V. Shuryak. Quark induced correlations between instantons drive the chiral phase transition. *Phys. Lett. B*, 325:263–266, 1994.
- [68] Thomas Schäfer, Edward V. Shuryak, and J. J. M. Verbaarschot. The Chiral phase transition and instanton - anti-instanton molecules. *Phys. Rev. D*, 51:1267–1281, 1995.
- [69] S. W. Hawking, I. G. Moss, and J. M. Stewart. Bubble Collisions in the Very Early Universe. *Phys. Rev. D*, 26:2681, 1982.
- [70] Bernard Carr and Florian Kuhnel. Primordial Black Holes as Dark Matter: Recent Developments. *Ann. Rev. Nucl. Part. Sci.*, 70:355–394, 2020.
- [71] Bernard Carr, Kazunori Kohri, Yuuiti Sendouda, and Jun’ichi Yokoyama. Constraints on primordial black holes. *Rept. Prog. Phys.*, 84(11):116902, 2021.
- [72] Tae Hyun Jung and Takemichi Okui. Primordial black holes from bubble collisions during a first-order phase transition. 10 2021.

- [73] M Yu Khlopov, RV Konoplich, SG Rubin, and Alexander S Sakharov. First order phase transitions as a source of black holes in the early universe. *arXiv preprint hep-ph/9912422*, 1999.
- [74] Christian T. Byrnes, Mark Hindmarsh, Sam Young, and Michael R. S. Hawkins. Primordial black holes with an accurate QCD equation of state. *JCAP*, 08:041, 2018.
- [75] Karsten Jedamzik. Primordial black hole formation during the QCD epoch. *Phys. Rev. D*, 55:5871–5875, 1997.
- [76] M. Joyce and Mikhail E. Shaposhnikov. Primordial magnetic fields, right-handed electrons, and the Abelian anomaly. *Phys. Rev. Lett.*, 79:1193–1196, 1997.
- [77] Kenji Fukushima, Marco Ruggieri, and Raoul Gatto. Chiral magnetic effect in the polyakov–nambu–jona-lasinio model. *Physical Review D*, 81(11):114031, 2010.
- [78] S. P. Klevansky and Richard H. Lemmer. Chiral symmetry restoration in the Nambu-Jona-Lasinio model with a constant electromagnetic field. *Phys. Rev. D*, 39:3478–3489, 1989.
- [79] K. G. Klimenko. Three-dimensional Gross-Neveu model in an external magnetic field. *Teor. Mat. Fiz.*, 89:211–221, 1991.
- [80] V. P. Gusynin, V. A. Miransky, and I. A. Shovkovy. Dimensional reduction and catalysis of dynamical symmetry breaking by a magnetic field. *Nucl. Phys. B*, 462:249–290, 1996.
- [81] G. S. Bali, F. Bruckmann, G. Endrodi, Z. Fodor, S. D. Katz, S. Krieg, A. Schafer, and K. K. Szabo. The QCD phase diagram for external magnetic fields. *JHEP*, 02:044, 2012.
- [82] G. S. Bali, F. Bruckmann, G. Endrodi, Z. Fodor, S. D. Katz, and A. Schafer. QCD quark condensate in external magnetic fields. *Phys. Rev. D*, 86:071502, 2012.
- [83] G. S. Bali, F. Bruckmann, G. Endrodi, F. Gruber, and A. Schaefer. Magnetic field-induced gluonic (inverse) catalysis and pressure (an)isotropy in QCD. *JHEP*, 04:130, 2013.
- [84] Chiara Caprini, Mark Hindmarsh, Stephan Huber, Thomas Konstandin, Jonathan Kozaczuk, Germano Nardini, Jose Miguel No, Antoine Petiteau, Pedro Schwaller, and G eraldine Servant. Science with the space-based interferometer elisa. ii: Gravitational waves from cosmological phase transitions. *Journal of cosmology and astroparticle physics*, 2016(04):001, 2016.
- [85] Sidney Coleman. Fate of the false vacuum: Semiclassical theory. *Physical Review D*, 15(10):2929–2936, 1977.
- [86] John Ellis, Marek Lewicki, and Jos e Miguel No. Gravitational waves from first-order cosmological phase transitions: lifetime of the sound wave source. *Journal of Cosmology and Astroparticle Physics*, 2020(07):050, 2020.
- [87] Pierre Bin etruy, Alejandro Boh e, Chiara Caprini, and Jean-Fran ois Dufaux. Cosmological backgrounds of gravitational waves and elisa/ngo: phase transitions, cosmic strings and other sources. *Journal of Cosmology and Astroparticle Physics*, 2012:027, 2012.
- [88] Astrid Eichhorn, Johannes Lumma, Jan M. Pawlowski, Manuel Reichert, and Masatoshi Yamada. Universal gravitational-wave signatures from heavy new physics in the electroweak sector. *Journal of Cosmology and Astroparticle Physics*, 2021:006, 2021.
- [89] Jose R Espinosa, Thomas Konstandin, Jose M No, and Geraldine Servant. Energy budget of cosmological first-order phase transitions. *Journal of Cosmology and Astroparticle Physics*, 2010(06):028, 2010.
- [90] Marc Kamionkowski, Arthur Kosowsky, and Michael S Turner. Gravitational radiation from first-order phase transitions. *Physical Review D*, 49(6):2837, 1994.
- [91] Mark Hindmarsh, Stephan J Huber, Kari Rummukainen, and David J Weir. Numerical simulations of acoustically generated gravitational waves at a first order phase transition. *Physical Review D*, 92(12):123009, 2015.
- [92] Christopher J Moore, Robert H Cole, and Christopher PL Berry. Gravitational-wave sensitivity curves. *Classical and Quantum Gravity*, 32(1):015014, 2014.
- [93] Wen-Hong Ruan, Zong-Kuan Guo, Rong-Gen Cai, and Yuan-Zhong Zhang. Taiji program: Gravitational-wave sources. *International Journal of Modern Physics A*, 35(17):2050075, 2020.
- [94] Jing Liu, Ligong Bian, Rong-Gen Cai, Zong-Kuan Guo, and Shao-Jiang Wang. Primordial black hole production during first-order phase transitions. *Physical Review D*, 105(2):L021303, 2022.
- [95] Tomohiro Harada, Chul-Moon Yoo, and Kazunori Kohri. Threshold of primordial black hole formation. *Physical Review D*, 88(8):084051, 2013.
- [96] Michael S. Turner, Erick J. Weinberg, and Lawrence M. Widrow. Bubble nucleation in first-order inflation and other cosmological phase transitions. *Phys. Rev. D*, 46:2384–2403, Sep 1992.
- [97] Dmitri E. Kharzeev. Chiral magnetic effect in heavy ion collisions and beyond. 4 2022.
- [98] Marek Lewicki and Ville Vaskonen. On bubble collisions in strongly supercooled phase transitions. *Physics of the Dark Universe*, 30, 2020.
- [99] M. Yu. Khlopov, R. V. Konoplich, S. G. Rubin, and A. S. Sakharov. First Order Phase Transitions as a Source of Black Holes in the Early Universe. *arXiv e-prints*, pages hep-ph/9912422, December 1999.
- [100] Karsten Jedamzik and Jens C Niemeyer. Primordial black hole formation during first-order phase transitions. *Physical Review D*, 59(12):124014, 1999.
- [101] Christian T Byrnes, Mark Hindmarsh, Sam Young, and Michael RS Hawkins. Primordial black holes with an accurate qcd equation of state. *Journal of Cosmology and Astroparticle Physics*, 2018(08):041, 2018.
- [102] JLG Sobrinho, P Augusto, and AL Gon alves. New thresholds for primordial black hole formation during the qcd phase transition. *Monthly Notices of the Royal Astronomical Society*, 463(3):2348–2357, 2016.